AD

CRDC-CR-84087

FLUID MOTION IN A ROTATING AND NUTATING CONTAINER

by THORWALD HERBERT

Department of Engineering Science and Mechanics
Virginia Polytechnic Institute and State University
Blacksburg, Virginia 24061

JULY 1984

US Army Armament, Munitions & Chemical Command
Aberdeen Proving Ground, Maryland 21010

Disclaimer

The findings in this report are not to be construed as an official Department of the Army position, unless so designated by other authorized documents.

Disposition

For classified documents, follow the procedures in DoD 5200.1-R, Chapter IX or or DoD 5220.22-M, "Industrial Security Manual," paragraph 19. For unclassified documents, destroy by any method which precludes reconstruction of the document.

Distribution Statement

Approved for public release; distribution unlimited.

UNCLASSIFIED

SECURITY CLASSIFICATION OF THIS PAGE

REPORT DOCUMENTATION PAGE

1a. REPORT SECURITY CLASSIFICATION UNCLASSIFIED	1b. RESTRICTIVE MARKINGS
2a. SECURITY CLASSIFICATION AUTHORITY	3. DISTRIBUTION / AVAILABILITY OF REPORT Approved for public release, distribution unlimited.
2b. DECLASSIFICATION / DOWNGRADING SCHEDULE	
4. PERFORMING ORGANIZATION REPORT NUMBER(S) CRDC-CR-84087	5. MONITORING ORGANIZATION REPORT NUMBER(S)
6a. NAME OF PERFORMING ORGANIZATION Dept. of Engineering Sci & Mechanics, Virginia Polytechnic Institute 6b. OFFICE SYMBOL (If applicable)	7a. NAME OF MONITORING ORGANIZATION
6c. ADDRESS (City, State, and ZIP Code) Blacksburg, VA 24061	7b. ADDRESS (City, State, and ZIP Code)
8a. NAME OF FUNDING / SPONSORING ORGANIZATION Chemical R&D Center 8b. OFFICE SYMBOL DRSMC-CLJ-IR (A)	9. PROCUREMENT INSTRUMENT IDENTIFICATION NUMBER DAAG29-81-D-0100
8c. ADDRESS (City, State, and ZIP Code) Aberdeen Proving Ground, MD 21010-5423	10. SOURCE OF FUNDING NUMBERS PROGRAM ELEMENT NO. / PROJECT NO. 1L161102 / TASK NO. A71A / WORK UNIT ACCESSION NO.

11. TITLE (Include Security Classification)

Fluid Motion in a Rotating and Nutating Container

12. PERSONAL AUTHOR(S)
Herbert, Thorwald

13a. TYPE OF REPORT	13b. TIME COVERED	14. DATE OF REPORT (Year, Month, Day)	15. PAGE COUNT
Contractor	FROM Jul 82 TO Jan 83	1984 July	52

16. SUPPLEMENTARY NOTATION

COTR: Miles Miller, DRSMC-CLB-PA (A) (301) 671-2186

17. COSATI CODES			18. SUBJECT TERMS (Continue on reverse if necessary and identify by block number)
FIELD	GROUP	SUB-GROUP	
15	02		Projectile stability
20	04		Liquid payloads
			Aeroballistics

19. ABSTRACT (Continue on reverse if necessary and identify by block number)

This report describes the initial phase of a study of the fluid motion in a container that is spinning and nutating. The moments exerted by this fluid motion on the container have been demonstrated to cause serious flight instabilities of shells with liquid payloads. The initial phase of our study concentrates on the relevant dimensionless parameters and equations that govern the fluid motion. Various special cases are discussed. Our analysis and aims at supporting ongoing experiments at Chemical Systems Laboratory (CSL)* and Ballistics Research Laboratory (BRL) and at providing a link between measurements of despin moments and side moments. It also prepares for an in-depth analysis of the interior flow field for comparison with flow visualizations at CRDC.

*Now the Chemical Research and Development Center (CRDC), US Army Armament, Munitions, and Chemical Command.

20 DISTRIBUTION / AVAILABILITY OF ABSTRACT	21. ABSTRACT SECURITY CLASSIFICATION
☒ UNCLASSIFIED/UNLIMITED ☐ SAME AS RPT ☐ DTIC USERS	UNCLASSIFIED
22a. NAME OF RESPONSIBLE INDIVIDUAL BRENDA C. ECKSTEIN	22b. TELEPHONE (Include Area Code) (301) 671-2914 / 22c. OFFICE SYMBOL DRSMC-CLJ-IR (A)

DD FORM 1473, 84 MAR 83 APR edition may be used until exhausted. All other editions are obsolete.

SECURITY CLASSIFICATION OF THIS PAGE
UNCLASSIFIED

BLANK

PREFACE

The work described in this report was authorized under Project No. 1L161102A71A, CB Defense Research. This work was started in July 1982 and completed in January 1983.

The use of trade names in this report does not constitute an official endorsement or approval of the use of such commercial hardware or software. This report may not be cited for purposes of advertisement.

Acknowledgments

Major parts of the reported work were supported under the Scientific Services Program, Contract No. DAAG29-81-D-0100, Delivery Order No. 0284 conducted between July 1982 and January 1983; COTR Miles C. Miller, Chemical Research and Development Center, Aberdeen Proving Ground, Maryland 21010-5423. Additional work was supported by the US Army Research Office, Mathematics Division, under Contract DAAG29-82-K-0129.

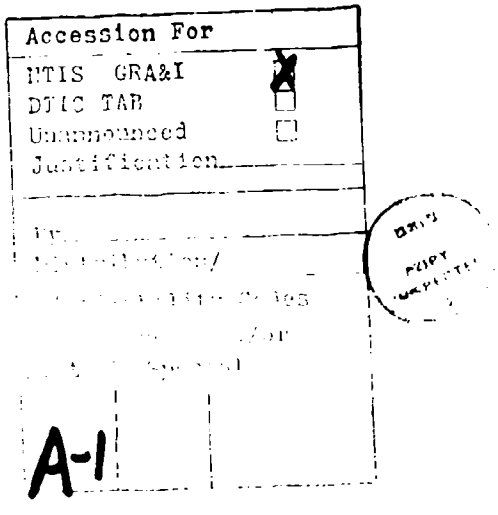

Blank

CONTENTS

FIGURES

TABLES

FLUID MOTION IN A ROTATING AND NUTATING CONTAINER

1. INTRODUCTION

Spin-stabilized projectiles with liquid payloads can experience severe flight instability. Instrumented flight tests indicate that this instability is characterized by a rapid increase in projectile yaw angle accompanied by an abrupt loss in spin rate. Detailed flight data for the XM761 smoke screening projectile were given by D'Amico.[1,2,3] These data clearly show that the instability is due to the motion of liquid white phosphorus embedded in cotton wicks; at lower ambient temperatures when the phosphorus is in a solid state, the projectile experiences a stable flight.

A laboratory test fixture was developed by Miller at CSL* to measure the despin moment of a full-scale XM761 container undergoing spinning and nutation.[4] Miller's tests[5,6] verified the suggestion of Vaughn[7] that white phosphorous in the wicks behaves like a homogeneous, very viscous fluid. The tests also revealed a maximum despin effect for fluids of kinematic viscosity in the range of 0.1 sq m/sec. Flight tests of projectiles having a container filled with corn syrup of kinematic viscosity 0.2 sq m/sec were conducted at BRL and showed instability very similar to that of the XM761.

The stability problem of the XM761 has, meanwhile, been overcome. The cotton wicks have been replaced by felt wedges, and separated by a longitudinal baffle and impermeable plastic foil. In view of future designs, however, there is ongoing interest in the interior fluid motion in spinning and nutating containers. The experiments at CSL have significantly simplified the research target by showing that the basic phenomena can be studied for homogenous liquid fills. The experiments have also shown that viscosity plays an important, if not dominating, role in the

*Now the Chemical Research and Development Center, US Army Armament, Munitions, and Chemical Command.

problem and this observation makes the study of the fluid motion a difficult task. Not only is an additional parameter introduced, but moreover, the theoretical analysis of the motion cannot resort to the simpler formulations of inviscid theory or boundary-layer theory.

Major efforts to reveal the fluid motion and to determine the despin and side moments required for aeroballistic investigations have been purely experimental. Miller conducted void observations in a transparent cylinder.[8] He also developed an improved spin fixture that allows for extended despin moment measurements as well as for flow visualizations using a laser-induced colored dye technique.[9] D'Amico and Rogers located liquid-filled containers within the rotor of a freely gimballed gyroscope and measured yaw growth rates at fixed spin rates.[10] The yaw growth indicates the side moment exerted by the liquid motion. Observations with highly viscous fluids showed that the growth rates were inconsistent with the predictions based on the resonant interaction with inertial oscillations as they occur in low-viscosity fluids.[11,12] Although the measurements of despin moments and yaw growth rates lead to consistent conclusions concerning the role of viscosity, they provide two completely separate sets of data. The link between these sets is given by the internal flow field in terms of velocity and pressure distribution. This flow field, however, is as yet unknown.

A first step into linking and better understanding the available data is to identify the nondimensional parameters that model the flow. The experimental data base is as yet too small to definitely identify these parameters, in particular the Reynolds number. We, therefore, resort to formal dimensional analysis and to an analysis, of governing equations and special solutions. The availability of the relevant parameters also efficiently supports the experiments since the amount of data recording can be drastically reduced and (future) experiments can be carried out with properly scaled containers, spin and nutation rates, and scaled working fluids.

The second step is to set up the governing equations in the best-suited coordinate system and to prepare for approximate solutions. Theoretical work in this direction is mostly based on the Stewartson-Wedemeyer approach, using an inviscid core flow that interacts with the boundaries through viscous boundary layers. Essential improvements have been achieved by Murphy and Gerber,[13] Sedney and Bartos.[14] Use of the boundary-layer approximation, however, precludes application of these theories and validity of their results at low Reynolds numbers. The restriction to small deviations from solid body rotation is always necessary for working with linearized equations. We consider various sets of linearized equations and discuss the inherent assumptions in relation with estimates from experimental data. In special cases, more general solutions or new insight into the structure of the motion is obtained. Finally, we discuss some aspects of computational methods for solving the complete equations.

2. EXPERIMENTAL APPROACH AND RESULTS

Before going into analysis, we briefly describe the experimental methods, the range of parameters, and the results obtained to date.

2.1 Despin Moment.

Measurements of the despin moment were conducted using a test fixture at CSL described by Miller.[4] A full-scale XM761 payload canister was mounted in a frame under an angle θ to the vertical axis. The canister was cylindrical, with inner radius $a = 60.3$ mm, length $2c = 517.6$ mm, and a total mass of about 12.25 kg. The angle θ could be varied to be 5, 10, 15, or 20 degrees. The cylinder was spun up by an air turbine to realistic spin rates of $\omega \leq 6000$ rpm. Then, the frame was rotated about its vertical axis up to the desired nutation rate of $\Omega \leq 600$ rpm. At higher nutation angles, the spin rate started to decrease before the frame reached high nutation rates (Miller,

private communication, 1982). After cutting off the air turbine, the spin rate was recorded as a function of time. The total despin moment was obtained as the product of spin deceleration and axial moment of inertia. The liquid-induced moment was found by subtracting the moment due to friction that was previously determined. As a result, the liquid-induced despin moment is given as function of Ω, ω, and θ. The method implies the following assumptions:

a. The nutation rate is constant during spin-down.

b. The motion of the liquid fill has no effect on the moment due to friction as a function of Ω, ω, and θ.

c. The fluid motion is quasi-steady; i.e., the spin-down is slow enough for the fluid motion to fully adapt to the instantaneous spin rates.

d. The friction moments are not a function of time.

For sufficiently high spin rates ($\omega \geq 1000$ rpm), the liquid moment was found to be independent of ω. Data for the XM761 payload are given in Miller's figures 7 to 9.[6] Additional data were obtained for the cylindrical container filled with homogeneous liquids of kinematic viscosities in the range from $\nu = 10^{-6}$ sq m/sec (water) up to 1.35 sq m/sec (corn syrup). These data are shown in figures 12 to 14 of the same paper. No attempt was made to measure the side moment exerted by the fluid, which would tend to increase the nutation (or yaw) angle θ. Only one aspect ratio, c/a = 4.29, of the cylinder was studied in these experiments.

An improved test fixture is presently in operation and more detailed data will soon be available.

2.2 Yaw Angle Growth Rate.

Measurements of the yaw angle growth rate using a gyroscope whose rotor contained a liquid-filled cylindrical cavity were conducted by Karpov,[15] Scott and D'Amico[16], and D'Amico and Rogers.[10] The nutation rate of the (empty) rotor for a given spin rate was varied by changing the moments of inertia. The rotor was spun up with the axis held fixed, and time was allowed for the fluid to reach a state of solid-body rotation. After releasing the gyroscope, the spin rate was held constant. The yaw angle was measured in terms of an amplitude, A, and ln A was recorded as a function of time.

The earlier experiments in the range of high Reynolds numbers served to verify Stewartson's theory. Linear increase of ln A with time (constant yaw growth rates) was found in some range of small yaw angles. Scott and D'Amico observed nonlinearity at angles as low as 1 degree (for $c/a \approx 3$). Virtually, a changeover to a constant growth rate occurred. At higher viscosity, the changeover still occurred but at higher yaw angles. The experiments of D'Amico and Rogers were made with silicone oils of high viscosity and with cylinders of aspect ratios $c/a = 3.126$ and 1.042. Spin rates were in the range of 3000 rpm. Constant yaw angle growth rates were found up to the limit of the apparatus at 5 degrees. The growth rates at a low Reynolds number turned out to be proportional to the nutation frequency and, therefore, must be due to a mechanism different from the Stewartson-Wedemeyer model. The data were correlated with various dimensionless parameters; however, a simple parametric dependence was not found.

The relation of the yaw angle growth rate to the moments exerted by the liquid is not easily obtainable. The moments of inertia are not given for the various data points, precluding determination of the side moment via the coefficients of the stability equation. Neither the inplane moment nor the despin moment have been separately measured. Therefore, the data are

completely separated from those in 2.1. They lead, however, to the same conclusion, that a basically viscous mechanism can lead to the instability of a projectile with liquid payload.

2.3 Flow Field.

The flow field that develops from the viscous fluid motion is unknown. Miller reported void observations for a (95%) filled cylinder with an aspect ratio of 4.45.[8] Due to the high spin rate (ω = 4000 rpm) the void was axisymmetric for solid-body motion. A characteristic wavy distortion of the void occurred when:

a. The nutation rate Ω was increased at fixed ν and θ,

b. The nutation angle θ was increased at fixed ν and θ,

c. The kinematic viscosity was decreased at fixed θ and Ω.

For low viscosity, the void was irregular, indicating turbulent fluid motion. The distortion was essentially restricted to the plane spanned by the spin axis and nutation axis. A similar observation was sketched by Scott's figure 1 without giving any detail.[17] Whereas Scott indicated that the void offset from the axis at the cylinder end plates, Miller's photographs show no offset. The effect of the void on the fluid motion is unknown.

Flow field observations are presently in preparation at CSL.[9] A laser-induced colored dye technique combined with high-speed photography is utilized to determine the three-dimensional velocity field.

3. DIMENSIONAL ANALYSIS

We consider a cylinder of length 2c and a radius a, rotating about its axis with the spin rate ω. The axis of the

cylinder is inclined to the (vertical) nutation axis by the nutation angle θ and rotates with nutation rate Ω about the vertical. The cylinder is completely filled with a fluid of constant density ρ and kinematic viscosity ν. The cylinder is symmetric with respect to the margin 0 defined by the point of intersection of the two axes of rotation (see figure 1).

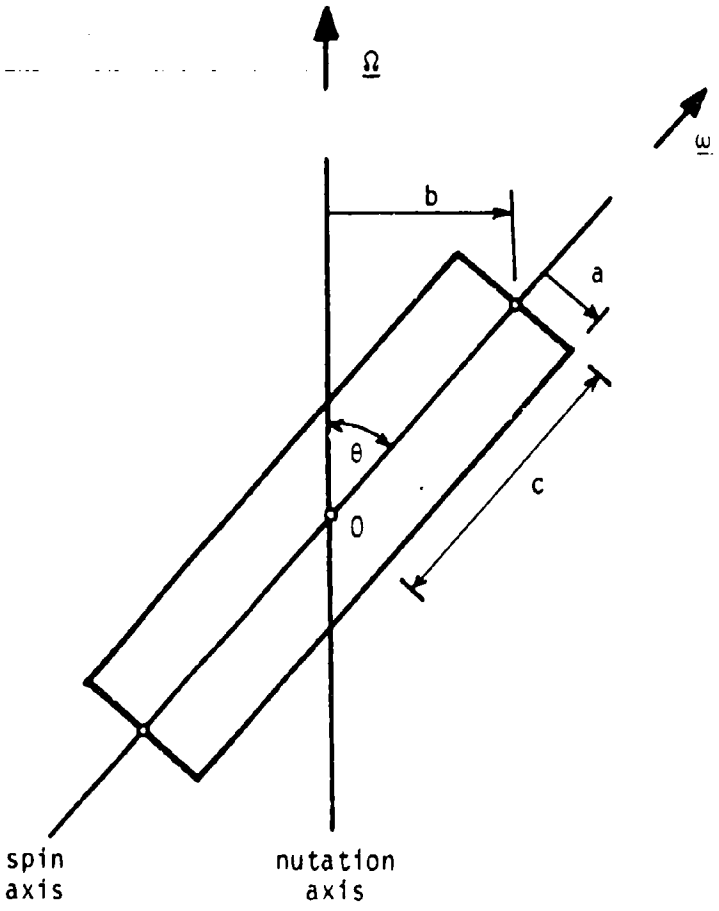

Figure 1. Dimensional Analysis Test Cylinder Configuration

The motion of the fluid is governed by the continuity equation

$$\nabla \cdot \underline{V} = 0 \qquad (1)$$

and the Navier-Stokes equations

$$\frac{D\underline{V}}{Dt} = -\frac{1}{\rho}\nabla p + \nu\nabla^2 \underline{V} \tag{2}$$

where $\underline{V}$ is the velocity vector and p the pressure. The $\underline{V}$ in equation (2) is measured in an inertial coordinate system. The body force due to gravity g is neglected in equation (2). Justification will be given shortly. Equations (1) and (2) are subject to the no-slip and no-penetration conditions at the side wall and end walls of the cylinder.

The solution of equations (1) and (2) under the given boundary conditions is completely determined when the following quantities are given: a, c, θ, ω, Ω, ρ, and ν. Hence, any quantity derived from this solution can be written as a function of these seven parameters. As an example, we write the despin moment M exerted by the flow at the cylinder as

$$M = f(a, c, \theta, \omega, \Omega, \rho, \lambda) \tag{3}$$

The principle of dimensional homogeneity requires that the function of f has the dimension of the moment M. According to Buckingham's Π-theorem, this can only be satisfied if the function of f is composed of terms that are products of powers of the seven parameters.[18] For example,

$$f_1 = \text{const } (a)^{p_1} (c)^{p_2} (\theta)^{p_3} (\omega)^{p_4} (\Omega)^{p_5} (\rho)^{p_6} (\nu)^{p_7} \tag{4}$$

where the constant is dimensionless and $p_1,\ldots,p_7$ are constant powers to be determined. We utilize the following dimension table:

	M	a	c	θ	ω	Ω	ρ	ν
Length (L)	2	1	1	0	0	0	-3	2
Time (T)	-2	0	0	0	-1	-1	0	-1
Mass (m)	1	0	0	0	0	0	1	0

which expresses, for example, the dimension of M as $m \cdot L^2/T^2$. Exploiting dimensional homogeneity of equation (4) and comparing powers of L, T, and m separately provides the following system of equations for $p_1,\ldots,p_7$:

$$L: \quad 2 = p_1 + p_2 - 3p_6 + 2p_7 \tag{5a}$$

$$T: \quad -2 = -p_4 - p_5 - p_7 \tag{5b}$$

$$m: \quad 1 = p_6 \tag{5c}$$

Since only three equations are available to relate the seven quantities, we are left with 4 degrees of freedom that express:

a. The presence of the nondimensional nutation angle θ

b. The presence of two length scales, a and c

c. The presence of two time scales, $1/\omega$ and $1/\Omega$

d. The possibility of defining an additional length scale (for example, a^2/ν) or time scale (for example, $a/\sqrt{\omega\nu}$) based on the kinematic viscosity.

Only equation (5c) provides unambiguously $p_6 = 1$, since there is a unique scale for the mass. Eliminating p_6 from equation (5a) results in

$$L: \quad 5 = p_1 + p_2 + 2p_7 \tag{5d}$$

In order to remove the ambiguity, we choose a, ω, and ρ to form a basic system of dimensions. We can then express equation (4) in the form

$$f_1 = \text{const} \cdot (a)^{p_1+p_2+2p_7} \quad (\omega)^{p_4+p_5+p_7}$$

$$(\rho)^{p_6} \left(\frac{c}{a}\right)^{p_2} \theta^{p_3} \left(\frac{\Omega}{\omega}\right)^{p_5} \left(\frac{\nu}{\omega a^2}\right)^{p_7}$$

where the powers of a, ω, and ρ are determined by equations (5d), (5b), and (5c), respectively. Introducing the dimensionless groups

$$\begin{aligned} \lambda &= c/a \text{ (aspect ratio)} \\ \tau &= \Omega/\omega \text{ (nutation frequency)} \\ \sigma &= \sin\theta \\ \mathrm{Re} &= \omega a^2/\nu \text{ (Reynolds number)} \end{aligned} \tag{6}$$

we obtain

$$f_1 = \text{const} \cdot \rho\omega^2 a^5 \left(\lambda^{p_2} \cdot \theta^{p_3} \cdot \tau^{p_5} \mathrm{Re}^{p_7}\right) \tag{7}$$

where the expression in parenthesis is dimensionless and the powers p_2, p_3, p_5, and p_7 are arbitrary. Forming the dimensionless despin moment M^*, we obtain from equations (3) and (7) in general form

$$\frac{M}{\rho\omega^2 a^5} = M^* = M^*(\mathrm{Re}, \lambda, \tau, \sigma) \tag{8}$$

In a completely analogous manner, we can form other dimensionless flow quantities with the functional dependence on the same

parameters (see equation 6). Different ways to find the functional dependence will be discussed in Section 3.2.

If partially filled cylinders were to be considered, the list of parameters (equation 6) had to be completed by the fill ratio = (fluid volume)/(volume of the cylinder). If gravity, g, were taken into account, the Froude number, $Fr = \omega^2 a/g$, would have to be included in the list of parameters. In our application, Fr is typically of the order 10^3--the inertial and/or viscous forces dominate the fluid motion. The negligible effect of the Froude number is clearly demonstrated by the cylindrical free surface in Miller's void observations (see figures 3a, 4a, and 5d).[8] This surface should be an axisymmetric paraboloid, if gravity had an effect. Anyway, if the fluid boundaries are fixed, as in the case of a completely filled cylinder, the Froude number is insignificant, and the only effect of gravity is to contribute a hydrostatic distribution to the pressure.

The definition of the Reynolds number in equation (6) is as arbitrary as the choice of the basic scales a and ω. Other Reynolds numbers can be derived:

$$Re_1 = Re \cdot \tau, \quad Re_2 = Re \cdot \tau \cdot \lambda^2, \quad Re_3 = Re \cdot \tau (\lambda\sigma)^2 \qquad (9)$$

or in terms of physical parameters

$$Re_1 = \Omega a^2/\nu, \quad Re_2 = \Omega c^2/\nu, \quad Re_3 = \Omega b^2/\nu \qquad (10)$$

where $b = c \cdot \sin\theta$ is the nutation radius of the cylinder (see figure 1). The question, which of these Reynolds numbers is most convenient, that is, leads to the simplest functional relation for M^* and so on, cannot be answered by the present formal dimensional analysis.

3.1 Formal Scaling Aspects

There are two important consequences of this dimensional analysis, however. First, we have reduced the number of seven physical parameters by the number of three basic dimensions to only four dimensionless parameters. This simplifies the mapping of the parametrical dependence. Second, equations such as (8) show that the nondimensional flow quantities are identical if Re, λ, τ, and σ are identical, no matter how these values are achieved. This fact allows working with properly scaled physical quantities.

Let us replace the original parameters a, c,..., by the model parameters $a_m = a \cdot \alpha_a$, $c_m = c \cdot \alpha_c$,..., where α_a, α_c,..., are scale factors. Then, a physically similar solution (identical in nondimensional terms) is obtained if the four parameters (equation 6) remain unchanged. In other words, if

$$\alpha_c = \alpha_a \tag{10a}$$

$$\alpha_\Omega = \alpha_\omega \tag{10b}$$

$$\alpha_\omega \cdot \alpha_a^2 = \alpha_\nu \tag{10c}$$

$$\alpha_\theta = 1 \tag{10d}$$

This last equation shows that the nutation angle (as a dimensionless quantity) cannot be scaled. With equation (10) satisfied, the same value of $M_m^* = M^*$ will be obtained according to equation (8). The physical (dimensional) moment, however, will change as

$$M_m = \alpha_\rho \alpha_\omega^2 \alpha_a^5 \cdot M \tag{11}$$

The relations (equations 10 and 11) allow model tests without any more detailed knowledge of the physics of the problem. It is

mainly equation (10c) that allows for changes of rotation rates, size of the cylinder, and viscosity of the liquid.

3.1.1 Scaled Container.

The experiments reviewed in Section 2.1 typically use a full-scale container with a mass of 12.25 kg, rotate it at 5000 rpm (10,000 rpm in the new test fixture), and impose a nutation with 500 rpm under an angle of up to 20 degrees. Clearly, operating this experiment bears the danger of catastrophic failure and, therefore, requires extreme care in designing, machining, and balancing the apparatus. The reason is obvious from equation (7) or (11): the moments increase with the fifth power of the length and with the second power of the rotation rates. The scaling relations (equation 10) allow the design of a harmless, smaller test fixture at reduced cost that bears other advantages.

Let us first consider that the working fluid remains unchanged, ($\alpha_\rho = 1$, $\alpha_\nu = 1$). If the linear dimensions of the cylinder are reduced by a factor of $\alpha_a < 1$, equation (10c) immediately requires $\alpha_\omega = 1/\alpha_a^2$, an increase of the rotation rates by a factor $1/\alpha_a^2$. From equation (11) it becomes clear that the moments are only reduced by a factor α_a. A drastic reduction of the moments cannot be achieved in this manner, since the required rotation rates would be prohibitive. It seems necessary, therefore, to change the working fluid. For liquids, there will be only a small variation in density, $\alpha_\rho = 1$, and the variation will be mainly in the viscosity. Keeping the original rotation rates, $\alpha_\omega = 1$ (equation 10c) requires $\alpha_\nu = \alpha_a^2$. Using a model with $\alpha_a = 1/2$, say, a liquid with $\nu_m = \nu/4$ must be used to maintain dynamical similarity. In view of the high viscosities of interest, such a liquid can easily be found. The moments, then, are considerably reduced by a factor $\alpha_\rho \alpha_a^5 \approx 1/32$. Further reductions can be achieved by the use of even smaller models.

3.1.2 Scaled Velocities of Working Fluids.

Disregarding structural problems, scaling may have other benefits, (for example, flow visualizations). Should it turn out that the velocities are too large for easy visualization of the colored dye, the time scale of the phenomena in the full-size cylinder can be changed by reducing spin rate, nutation rate, and viscosity by the same factor, $\alpha_\omega = \alpha_\Omega = \alpha_\nu$. The moments drop by $\alpha_\rho \alpha_\omega^2$, slowing down the spin-down process. The velocities drop by the factor α_ω. Smaller picture frequency (factor α_ω) and larger exposure times (factor $1/\alpha_\omega$) would recover the original results. Should it be desirable to work with a special fluid, for example, water instead of some more viscous silicone oil, the necessary adjustments of rotation rates and cylinder size can be made according to $\alpha_\nu = \alpha_a^2 \alpha_\omega$, from equation (10c).

3.1.3 A Small Model Test Fixture.

By proper choice of the scale factor α, it seems possible to set up a model test fixture (based on a standard record player as a turntable) at low cost for direct visual observation of the motion in high-viscosity fluids. With fixed $\Omega_m = 45$ rpm, the range of nutation rates can be covered with $\alpha_\omega > 0.075$. A reasonable range of τ can be obtained with $\omega_m < 2000$. With $\alpha_a = \alpha_c = 0.4$, the filled model cylinder has a mass of approximately 0.8 kg. Moments are reduced by about four orders of magnitude. The resulting factors $\alpha_\nu > 0.012$ allow covering the interesting range of higher viscosities.

3.1.4 Data Reduction and Cross-Checks.

Miller's experiments at CSL provide despin moments for fixed $\lambda = c/a$, for four values of $\sigma = \sin\theta$, and numerous values of the viscosity. Nutation rates can be varied in a broad range, and spin rates vary continuously during spin-down. It is obvious from equation (8) that only two parameters, Re and τ, need to be varied

to obtain (or document) the complete parametric dependence of M^* for fixed λ and σ. It is useful, therefore, to present all data in dimensionless form. The experimental procedure mentioned earlier partially duplicates data. As an example, nutation rates Ω_1 and $\Omega_2 = \Omega_1/2$ with fluids of viscosities ν_1 and $\nu_2 = \nu_1/2$ should provide identical values of M^* at ω_1 and $\omega_2 = \omega_1/2$. This duplication can be utilized for a cross-check of the data and for verifying the validity of the assumptions outlined in Section 2.1. With this validity assured, the duplication can be avoided in future experiments by using cylinders of different aspect ratios.

3.2 Parametrical Dependence.

The second step in the fluid motion analysis and the resulting moments requires finding the functional dependencies of nondimensional variables such as M^* in equation (8) on the parameters Re, λ, τ, and σ. The results can then be recast in terms of other, perhaps better suited parameters, such as one of the modified Reynolds numbers in equations (9) and (10). Various methods can be exploited and their results combined to achieve this goal:

- Physical arguments
- Analysis of experimental data
- Formal analysis of the governing equations
- Analysis of numerical results
- Analytical solutions.

Knowledge of the analytical solution for the velocity and pressure field would completely solve the problem. However, there is no chance to find the solution of the full Navier-Stokes equations. Simplifications that may permit finding approximate solutions will be discussed in Section 5. Numerical solutions of the full

equations can be obtained, in principle, but are not yet available. Analysis of the governing equations--even without solving them--sometimes reveals special combinations of the parameters as most relevant. An example is the Taylor number $Ta = 2Re^2 \cdot (R_2 - R_1)/(R_2 + R_1)$, with $Re = \Omega R_1(R_2 - R_1)/\nu$, that characterizes the fluid motion of a viscous liquid between concentric cylinders of radii R_2 and R_1, with the outer fixed and the inner rotating with Ω. Similar combinations, square of the Reynolds number times a purely geometric parameter, occur in other problems. Physical arguments are sparse in the present context and can be misleading, in fact, since the motions of rotating fluids are often beyond our imagination. In the following discussion, we attempt an analysis of the experimental data.

3.2.1 An Example: Despin Moments.

This analysis is heavily restricted by the small number of available data. These data are uncertain due to experimental errors that are yet known. (Estimates from the cross-checks suggested in Subsection 3.1.4 would be helpful.) Additional error is introduced by reading the data from small figures.

From Miller's figure 7, it appears that the despin moment M at fixed λ and σ varies proportionally to $\Omega^{2.6}$. Liquid density and viscosity are not easy to identify for the wick-type fill. We have therefore, not used M* but calculated M/Ω^2. The values of τ and of M/Ω^2 are given in table 1. There is only a small scatter in the values of M/Ω^2, largest for the data points with small values of M that are difficult to read accurately from the graphs. An average value of 1.77×10^{-3} Nms^2 is obtained such that

$$M \approx 1.77 \times 10^{-3} \Omega^2 \text{ or } \frac{M}{\omega^2} \approx 1.77 \times 10^{-3} \tau^2 \qquad (12)$$

where Ω or ω are in radians/sec. Based on runs 74 and 25 only, the average value would be smaller, 1.71×10^{-3} $N \cdot m \cdot sec^2$.

Table 1. Despin Moments Analysis Data*

Run	ω	Ω	τ	M	10^3 M/Ω^2
	(rpm)	(rpm)		(N · m)	(N · m · sec^2)
74	1000	381	0.381	2.56	1.61
	1250	379	0.303	2.69	1.71
	1500	366	0.244	2.70	1.84
	2000	347	0.174	2.33	1.76
	3000	299	0.0997	1.60	1.63
	4000	225	0.0564	0.895	1.61
	4500	159	0.0354	0.479	1.73
25	1500	354	0.236	2.34	1.70
	2000	339	0.170	2.26	1.79
	3000	293	0.0977	1.61	1.71
	4000	221	0.0553	0.947	1.77
23	2500	296	0.118	1.71	1.78
	4000	192	0.0479	0.652	1.61
	4500	100	0.0222	0.289	2.64
26	2000	192	0.0958	0.698	1.73
	2500	107	0.0427	0.277	2.21
21	2000	156	0.0780	0.393	1.47
	2500	101	0.0403	0.173	1.55

*Extracted from Miller's Figure 7.[6]

The deviation from this average is shown in figure 2. It is difficult to decide on a systematic variation with ω [or the Reynolds number (Re)]. Although there seems to be a tendency for the data of these two runs, we refrain from any additional conclusion.

From Miller's figures 8 and 9, the effect of θ or σ can be estimated. The values of M/Ω^2 for the four angles θ are given in table 2. It turns out that the ratio of $M/(\Omega \sin \theta)^2$ is almost the same for each of the four angles. Significant deviation occurs only for $\theta = 5$ degrees. For $\theta > 5$ degrees, the data can be approximated by

$$M \simeq 0.0156(\Omega \sin \theta)^2 \text{ or } \frac{M}{\omega^2} \simeq 0.0156(\tau\sigma)^2 \qquad (13)$$

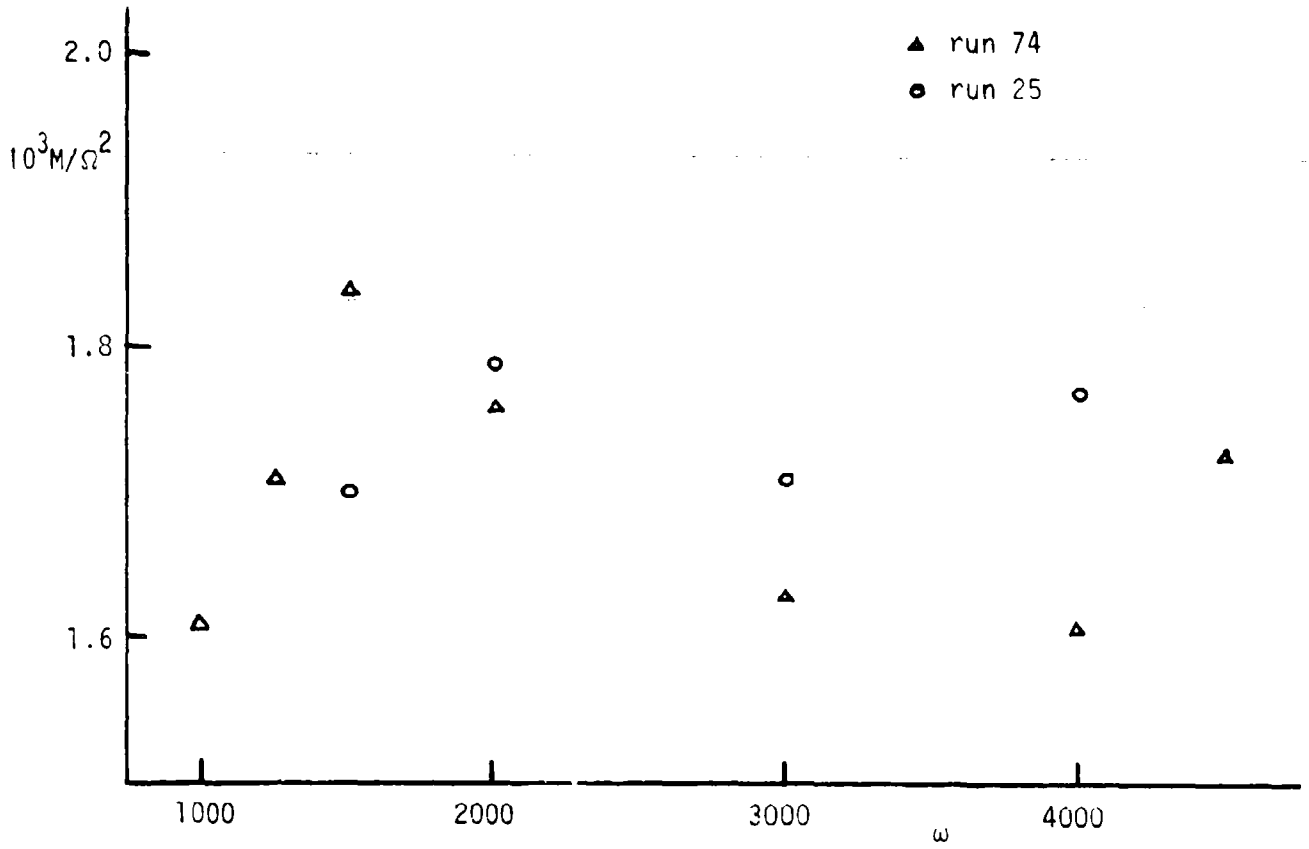

Figure 2. Deviation from the Average Value Based on Runs 74 and 25

Table 2. Values of M/Ω^2 for the Four θ Angles*

θ	σ = sin θ	10^3 M/Ω^2	$M/(\Omega \sin \theta)^2$	Average
(degrees)		(N · m · sec^2)	(N · m · sec^2)	
5	0.0872	0.076	0.0100	
10	0.1736	0.497	0.0165	0.0156
15	0.2588	1.02	0.0153	
20	0.3420	1.77	0.151	

*From Figures 8 and 9 of Miller[6]

A similar approximation can be obtained from the data in table 3 for Miller's figure 12. In this case, the cylinder is filled with a homogeneous fluid of high viscosity. Combining data for all four angles θ results in

$$M \approx 0.00814(\Omega \sin \theta)^2 \qquad (14)$$

The different constants in equations (13) and (14) can be attributed to various effects: different mass of liquid, different effective viscosity, and, in addition, different geometry due to the baffle in the wick-type payload.

Table 3. Approximation of Miller's[6] Data with the Cylinder Filled with a Homogeneous Fluid of High Viscosity*

θ (degrees)	$\sigma = \sin \theta$	$10^3 M/\Omega^2$ ($N \cdot m \cdot sec^2$)	$M/(\Omega \sin \theta)^2$ ($N \cdot m \cdot sec^2$)	Average
5	0.0872	0.0689	0.00904	0 00814
10	0.1736	0.2116	0.0070	
15	0.2588	0.5559	0.00830	
20	0.3420	0.9581	0.00819	

*Miller's Figure 12[6]

The expressions for M contain only quantities that are related to nutation. This reflects Miller's observation that the despin moment was essentially independent of the spin rate whenever ω was sufficiently large. The other parameters, in particular those that were held constant, are hidden in the constants. The aim of finding the functional relation [see equation (8)] in an as-simple-as-possible form also requires reviewing the reference quantities that were chosen to obtain the parameters [see equation (6)]. Equations (13) and (14) suggest that the reference

velocity ωa should be replaced by $\Omega c \sin\theta$. From physical arguments, it also seems reasonable to replace ρa^3 by the effective mass of liquid, $m_\ell = 2\pi\rho a^2 c$, so that

$$M = m_\ell \, (\Omega c \sin\theta)^2 \cdot M_1^* \tag{15}$$

where $M_1^* = M^*/2(\pi\lambda^3\tau^2\sigma^2)$ is almost independent of Ω, ω, and θ.

The dependence of M_1^* on the viscosity can be estimated from Miller's figure 13.[6] Figure 3 shows a modified plot of these data in the form, log M versus log $1/\nu$. This representation has been chosen since ν appears only in the Reynolds number and, therefore, the dependence of M^* on Re should be revealed by this plot. Although only a few data points are available, it is obvious that at least two regions can be distinguished. For high viscosity (region I), $\nu \geq 0.2$ m^2/sec, it seems that $M_1^* \sim 1/\nu$, whereas for $\nu < 0.1$ m^2/sec (region II), the data align along $M_1^* \sim (1/\lambda)^{-0.32}$, with some transition region in between. It is not clear, though, whether a second transition occurs for $\nu \leq 10^{-4}$ m^2/sec.

The data of Miller's figure 12 and the moments according to equation (14) are located in the region where $M_1^* \sim 1/\nu$. Since Ω and θ are constant for figure 13 and ν is constant for figure 12, both sets of data can be combined into

$$M = m_\ell \Omega \frac{\Omega(c \sin\theta)^2}{\nu} M_2 = m_\ell \, \Omega \, \mathrm{Re}_3 \, M_2 \tag{16}$$

where M_2 is almost independent of Ω, ω, θ, and ν. From comparison with equation (14) we obtain

$$M_2 \approx 0.00294 \text{ m}^2/\text{sec} \tag{17}$$

The value of the Reynolds number for the data in figure 12 is $\mathrm{Re}_3 \approx 2.05$, very small indeed. For the range of smaller viscosities, expressions analogous to equation (16) cannot be

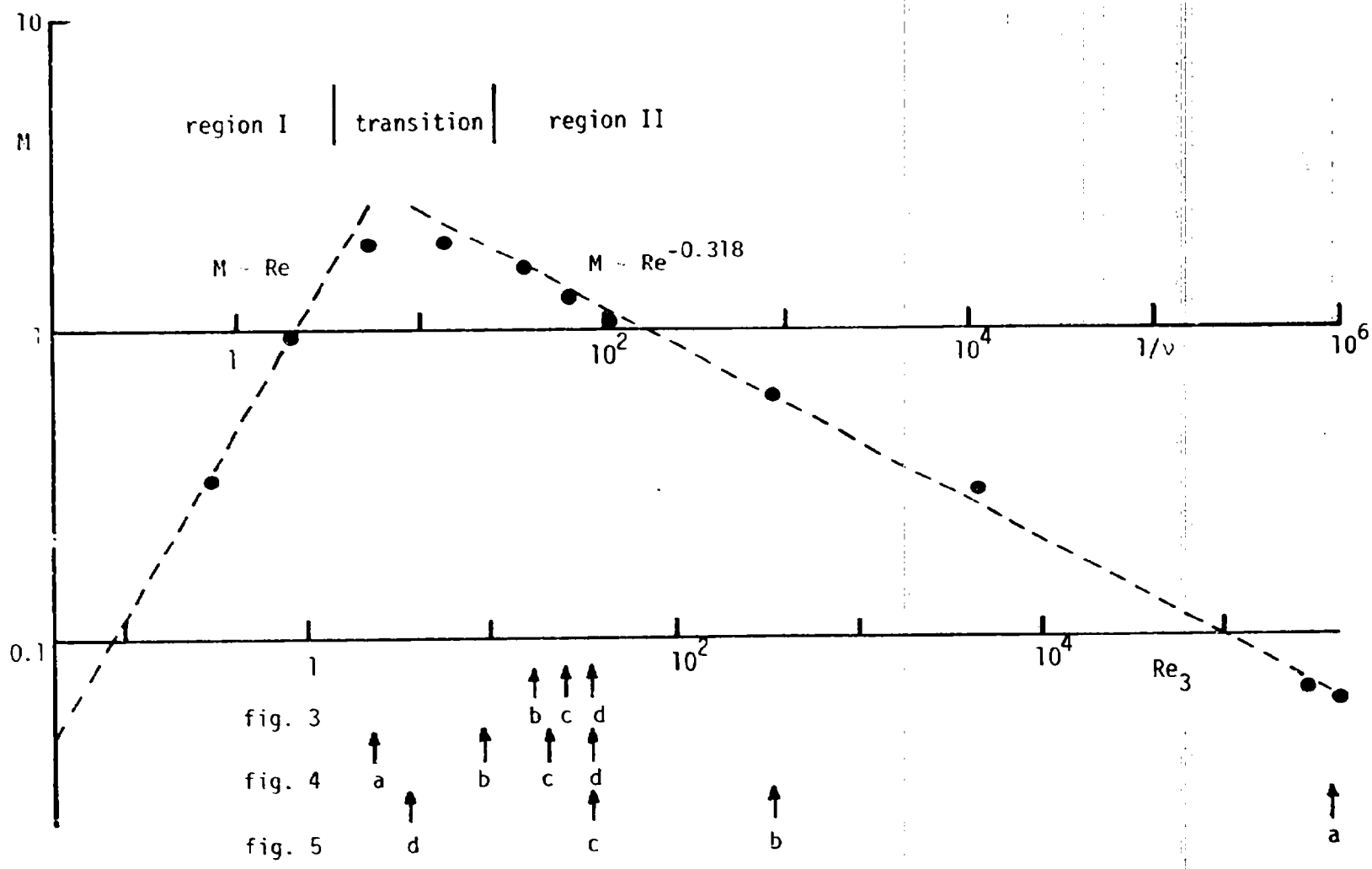

Figure 3. Modified Plot of Miller's Data (Figure 13[b])

derived due to the lack of data. We also note that the approximations suggested in this section need further verification.

If one adopts Re3 as the relevant Reynolds number, the void observations of Miller can be linked to the despin moments in figure 3.[8] The slight difference in the lengths of the cylinders can be neglected. The arrows in figure 3 indicate the Reynolds numbers for the photographs in Miller's figures 3, 4, and 5. To within the accuracy of reading the void distortion from the small reproductions, the value of Re3 sorts the pictures in the sequence of increasing amplitude of the sinusoidal distortion. The void distortion is barely visible in pictures 4a and 5b, but increases as Re3 changes through the transition region into region II. It is tempting, therefore, to associate the void distortion with the deviation of the despin moments from equation (16) for region I. One might also speculate that the motion in region I is essentially axisymmetric. Flow visualizations of the axial velocity component can decide this issue.

3.2.2 Gyroscope Data.

We attempted to exploit the measurements of D'Amico and Rogers in order to check the previous conclusions and to obtain additional insight.[10] However, this attempt failed since the inertial moments of the gyroscope are not given in the paper; these data are necessary for extracting the liquid side moments from the equations provided by the tri-cyclic theory.[19]

We also attempted to correlate the yaw angle growth rates with various dimensionless parameters. One of our observations seems worth reporting: If τ_i/Re is plotted versus τ_r, the (few) data points fit well on straight lines, in particular for the cylinder with $\lambda \approx 1$. The slope of these lines seems to be independent of ω, but increases with viscosity.

4. GOVERNING EQUATIONS

Since the experimental data base is too small for a detailed analysis of the moments exerted by the moving fluid, we prepare for complementary theoretical studies. This requires one to decide on a suitable coordinate system and to write the equations of fluid motion and appropriate boundary conditions in these coordinates. Subsequently, simplified sets of equations can be developed using various assumptions for approximate solutions.

The geometry and kinematics of our problem suggest one of the following three coordinate systems:

- Inertial or earth-fixed axes, index i
- Cylinder-fixed or body-fixed axes, index b
- Intermediate, nutation-oriented coordinate system, index n.

The choice of a special system is largely guided by the idea that the parameters of the problem should appear in the differential equations, not in the boundary conditions. The boundary conditions should be as simple as possible. These requirements are obviously not satisfied if equations (1) and (2) for an inertial system are used. Only ν and ρ appear in these equations, while the remaining five parameters are hidden in the boundary conditions. Moreover, the boundary conditions are time-dependent.

4.1 Coordinates Fixed to the Cylinder.

Coordinates fixed to the spinning cylinder are analogous to the body axes often used in aeroballistics. The velocity $\underline{V} = \underline{V}_i$ in equations (1) and (2) is measured with respect to an inertial system. The body-fixed system rotates with angular velocity $\underline{\Omega}_b$, where

$$\underline{\Omega}_b = \underline{\Omega}_b(t) = \underline{\Omega} + \underline{\omega}(t) \tag{18}$$

with respect to the inertial system, where $\underline{\Omega}$ and $\underline{\omega}$ point in the direction of the nutation axis and spin axis, respectively. In this system, a different velocity, $\underline{V}_b$, will be measured. Velocities $\underline{V}_i$ and $\underline{V}_b$ are related by

$$\underline{V}_i = \underline{V}_b + \underline{\Omega}_b \times \underline{r} \tag{19}$$

where $\underline{r}$ is the position vector.[20] This transformation leaves the continuity equation unchanged:

$$\nabla \cdot \underline{V}_b = 0 \tag{20}$$

Moreover, for a Newtonian fluid, the viscous terms are invariant under the transformation equation (19). Major changes occur only in the acceleration terms:

$$\frac{D\underline{V}_i}{Dt} = \frac{D\underline{V}_b}{Dt} + 2\underline{\Omega}_b \times \underline{V}_b + \underline{\Omega}_b \times (\underline{\Omega}_b \times \underline{r}) + \dot{\underline{\Omega}}_b \times \underline{r} \tag{21}$$

where $\dot{\underline{\Omega}}_b$ denotes the time-derivative of $\underline{\Omega}_b$. The three additional terms containing $\underline{\Omega}_b$ are the Coriolis acceleration, the centripetal acceleration, and the acceleration due to the change of the rotation rate, respectively. The centripetal acceleration can be written in terms of a potential function ϕ_c:

$$\underline{\Omega}_b \times (\underline{\Omega}_b \times \underline{r}) = -\nabla\phi_c \tag{22}$$

and can be considered as an additional (conservative) force per unit mass. Therefore, this term is written on the right-hand side of the momentum equation:

$$\frac{D\underline{V}_b}{Dt} + 2\underline{\Omega}_b \times \underline{V}_b + \dot{\underline{\Omega}}_b \times \underline{r} = -\frac{1}{\rho}\nabla p + \nabla\phi_c + \Omega\nabla^2\underline{V}_b \tag{23}$$

It is obvious from equation (23) that the centrifugal force can be combined with the pressure p into a reduced pressure:

$$p_b = p - \rho \Phi_c = p - \frac{1}{2\rho} |\underline{\Omega}_b \times \underline{r}|^2 \tag{24}$$

The boundary conditions of no-penetration and no-slip reduce to the simple form

$$\underline{V}_b = 0 \text{ at the boundaries} \tag{25}$$

Only the radius a and the half-length c of the cylinder are introduced by equation (25). All the other parameters of the problem are contained in equation (23) with $\underline{\Omega}_b$ from equation (18). The system of equations (20) and (23), with (25), supports trivial solutions $\underline{V}_b \equiv 0$, $p_b \equiv 0$, whenever $\dot{\underline{\Omega}}_b = 0$ (that is, rigid-body motion of the fluid). In a more obvious form, this result can be written as

$$\underline{V}_b \equiv 0, \; p_b \equiv 0 \text{ for } \omega \Omega \sin\theta = 0 \tag{26}$$

There are, in fact, three separate cases of rigid-body motion:

- For zero spin rate, $\omega = 0$
- For zero nutation rate, $\Omega = 0$
- For a rotation with $\omega + \Omega$ about the same axis.

According to equation (24) $p_b = 0$ describes the pressure distribution

$$p = \frac{1}{2} \rho |\underline{\Omega}_b|^2 r_d^2 \tag{27}$$

where r_d is the distance from the axis of rotation.

A fourth case of rigid-body motion occurs for large viscosity, $\upsilon \to \infty$. In this limit, equation (23) reduces to $\nabla^2 \underline{v}_b = 0$ for Stokes flow.

4.1.1 Dimensionless Form.

Using the basic system of dimensions (a, ω, and ρ), we introduce dimensionless variables (denoted by $\hat{}$) in the following way:

$$\underline{r} = \hat{\underline{r}} \cdot a, \quad t = \hat{t}/\omega \tag{28}$$

$$\underline{V} = \hat{\underline{V}} \cdot a\omega, \quad \underline{\Omega}_b = \hat{\underline{\Omega}}_b/\omega, \quad p_b = \hat{p}_b \cdot \rho(a\omega)^2 \tag{29}$$

The basic equations then take the following form:

$$\nabla \cdot \hat{\underline{V}}_b = 0 \tag{30}$$

$$\frac{D\hat{\underline{V}}_b}{D\hat{t}} + 2\hat{\underline{\Omega}}_b \times \hat{\underline{V}}_b + \frac{d\hat{\underline{\Omega}}_b}{d\hat{t}} \times \hat{\underline{r}} = -\nabla\hat{p}_b + \frac{1}{Re} \nabla^2 \hat{\underline{V}}_b \tag{31}$$

In equation (31), ∇ refers to dimensionless variables.

We note that the spin rate ω must be nonzero for the availability as a reference quantity. This is no restriction, however, since according to equation (26) rigid-body motion occurs for $\omega = 0$. We are rather interested in the deviations from rigid-body motions for $\omega \neq 0$.

4.1.2 Components in Cylindrical Coordinates.

In view of the axisymmetry of the boundary, we introduce cylinder coordinates r, ϕ, and z, where the z-axis coincides with the cylinder axis and $r = 1$, $\phi = z = 0$ describes a fixed point of the cylindrical side wall. Since no further use is made of

dimensional variables, we simplify the notation by dropping the ^. Using equation (6), we obtain the components of $\underline{\Omega}_b$ and $\dot{\underline{\Omega}}_b$ in the form:

$$\Omega_r = -\tau\sigma \cos(t + \phi), \quad \dot{\Omega}_r = \dot{\Omega}_\phi$$

$$\Omega_\phi = \tau\sigma \sin(t + \phi), \quad \dot{\Omega}_\phi = -\Omega_r$$

$$\Omega_z = 1 + \tau(1 - \sigma^2)^{1/2}, \quad \dot{\Omega}_z = 0 \tag{32}$$

With $\underline{V}_b = (u_r, u_\phi, u_z)$, the continuity equation (30) yields

$$\frac{1}{r}\frac{\partial}{\partial r}(ru_r) + \frac{1}{r}\frac{\partial u_\phi}{\partial \phi} + \frac{\partial u_z}{\partial z} = 0 \tag{33}$$

while the momentum equations take the form

$$D'u_r - \frac{u_\phi^2}{r} - 2(\Omega_z u_\phi - \Omega_\phi u_z) + \dot{\Omega}_\phi z$$

$$= -\frac{\partial p_b}{\partial r} + \frac{1}{Re}\left(D''u_r - \frac{u_r}{r^2} - \frac{2}{r^2}\frac{\partial u_\phi}{\partial \phi}\right) \tag{34a}$$

$$D'u_\phi + \frac{u_r u_\phi}{r} + 2(\Omega_z u_r - \Omega_r u_z) - \dot{\Omega}_r z$$

$$= -\frac{1}{r}\frac{\partial p_b}{\partial \phi} + \frac{1}{Re}\left(D''u_\phi - \frac{u_\phi}{r^2} + \frac{2}{r^2}\frac{\partial u_r}{\partial \phi}\right) \tag{34b}$$

$$D'u_z + 2(\Omega_r u_\phi - \Omega_\phi u_r) - \dot{\Omega}_\phi r = -\frac{\partial p_b}{\partial z} + \frac{1}{Re} D''u_z \tag{34c}$$

where

$$D' = \frac{\partial}{\partial t} + u_r \frac{\partial}{\partial r} + \frac{u_\phi}{r} \frac{\partial}{\partial \phi} + u_z \frac{\partial}{\partial z}$$

and

$$D'' = \frac{\partial^2}{\partial r^2} + \frac{1}{r} \frac{\partial}{\partial r} + \frac{1}{r^2} \frac{\partial^2}{\partial \phi 2} + \frac{\partial^2}{\partial z^2}$$

The boundary conditions require

$$u_r = u_\phi = u_z = 0 \quad \text{for } r = 1, \ |z| \leq \lambda, \ 0 \leq \phi < 2\pi \qquad (35a)$$

$$u_r = u_\phi = u_z = 0 \quad \text{for } z = \pm\lambda, \ 0 \leq r \leq 1, \ 0 \leq \phi < 2\pi \qquad (35b)$$

Although these conditions are independent of time, a time-dependent solution is desirable, due to the time-dependence of the coefficients Ω_r, Ω_ϕ [see equation (32)]. It is obvious that a simple time-periodicity with period $T = 2\pi$ will evolve if transient behavior (after sudden start of nutation, for example) is disregarded.

The possibility of studying small deviations from rigid-body motion as a perturbation of the zero-state [see equation (26)] seems to support the use of this body-fixed coordinate system. The periodicity in time can be taken into account by introducing a modified azimuthal coordinate, $\phi' = \phi + t$. At closer analysis, however, this change of coordinates is equivalent to working in a system that rotates only with $\underline{\Omega}$ about the nutation axis.

4.2 Coordinates Fixed to the Axes of Rotation.

This nutating coordinate system rotates with constant angular velocity $\underline{\Omega}_n = \underline{\Omega}$ about the origin. The equations of Section 4.1 require little change: Quantities with index b are replaced by quantities with index n and the terms with $\dot{\underline{\Omega}}_n$ are dropped. The boundary conditions, however, are inhomogeneous, due to the rotation rate ω of the cylinder with respect to the nutating

system. Instead of equation (26), the trivial solutions for $\Omega \sin\Theta = 0$ are rigid-body rotations with ω about the cylinder axis. Homogeneous boundary conditions can be retrieved, and an apparently simple formulation can be obtained by splitting the velocity field $\underline{V}_n$ into a rigid-body rotation with ω and a deviation due to $\Omega \sin\Theta \neq 0$. In the following, we return to dimensionless variables.

We introduce cylindrical coordinates r, ϕ, and z, where the z-axis coincides with the cylinder axis, as before. However, $\phi = 0$ describes points in the plane spanned by the nutation axis and spin axis, because $\Theta \neq 0$. The components of $\underline{\Omega}_n = \underline{\Omega}$ are

$$\Omega_r = -\tau\sigma\cos\phi\,, \quad \Omega_\phi = \tau\sigma\sin\phi\,, \quad \Omega_z = \tau(1-\sigma^2)^{1/2} \tag{36}$$

Hence, in the nutating frame, the Coriolis acceleration introduces no explicit time-dependence.

4.2.1 Decomposition of the Flow Field.

We decompose the velocity $\underline{V}_n = (u_r, u_\phi, u_z)$ and the reduced pressure p_n according to

$$u_r = v_r,\ u_\phi = \Omega_\phi r + v_\phi,\ u_z = v_z$$

$$p_n = p' + \frac{1}{2}(1 + 2\Omega_z)\, r^2 \tag{37}$$

Although the continuity equation remains in the form

$$\frac{1}{r}\frac{\partial}{\partial r}(rv_r) + \frac{1}{r}\frac{\partial v_\phi}{\partial \phi} + \frac{\partial v_z}{z} = 0 \tag{38}$$

for the deviation (v_r, v_ϕ, v_z), the momentum equations take the following form:

$$D'v_r - \frac{v_\phi^2}{r} - 2(1 + \Omega_z)\, v_\phi + 2\Omega_\phi v_z$$

$$= - \frac{\partial p'}{\partial r} + \frac{1}{Re}\left[D''v_r - \frac{v_r}{r^2} - \frac{2}{r^2}\frac{\partial v_\phi}{\partial \phi}\right] \tag{39a}$$

$$D'v_\phi + \frac{v_r v_\phi}{r} + 2(1 + \Omega_z)\, v_r - 2\Omega_r v_z$$

$$= - \frac{1}{r}\frac{\partial p'}{\partial \phi} + \frac{1}{Re}\left[D''v_\phi - \frac{v_\phi}{r^2} + \frac{2}{r^2}\frac{\partial v_r}{\partial \phi}\right] \tag{39b}$$

$$D'v_z + 2\Omega_r v_\phi - 2\Omega_\phi v_r = - \frac{\partial p'}{\partial z} - 2r\Omega_r + \frac{1}{Re} D''v_z \tag{39c}$$

D' now reads:

$$D' = \frac{\partial}{\partial t} + \frac{\partial}{\partial \phi} + v_r \frac{\partial}{\partial r} + \frac{v_\phi}{r}\frac{\partial}{\partial \phi} + v_z \frac{\partial}{\partial z} \tag{40}$$

The boundary conditions are homogeneous:

$$v_r = v_\phi = v_z = 0$$

$$\text{for} \quad r = 1, \ |z| \leq \lambda, \ 0 \leq \phi < 2\pi \tag{41a}$$

$$v_r = v_\phi = v_z = 0$$

$$\text{for} \quad z = \pm\lambda, \ 0 \leq r \leq 1, \ 0 \leq \phi < 2\pi \tag{41b}$$

The system equations (38) through (41) for the deviation from rigid-body motion bears some advantages over equations (33) through (35). The system can support steady solutions; this formal conclusion is consistent with Miller's void observations, which showed a steady void distortion in the nutating system. This system can be

easily linearized and the conditions for linearization are obvious (see Section 5). Equation (39) displays an important forcing term, $2r\Omega_r = -2\tau\sigma r \cos\phi$, which cannot be incorporated into the reduced pressure. In dimensional form, this term is proportional to $\omega\Omega \sin\theta$. By comparison with equation (23), it becomes clear that this term produces the deviation. In fact, the system equations (38) through (41) have a trivial solution if, and only if, $Re \cdot \Omega_r = 0$. In the following sections, we continue the analysis based on the equations and notation introduced for the nutating system.

4.2.2 The Reduced Pressure p'.

The relation between the reduced pressure p_n and the pressure p is given by

$$p_n = p - \frac{1}{2}\left|\underline{\Omega}_n \times \underline{r}\right| = p - \frac{1}{2}\tau^2 \cdot r_d^2 \qquad (42)$$

where r_d is the distance from the nutation axis.

From equation (37) we obtain

$$p' = p - \frac{1}{2}\left[(1 + 2\Omega_z)\, r^2 + \tau^2 r_d^2\right] \qquad (43)$$

Using equation (36), we find for point r, ϕ, z

$$p' = p - \frac{1}{2}\left\{\left[1 + \tau(1 - \sigma^2)^{1/2}\right]^2 r^2 + (\tau\sigma r \sin\phi)^2 + (\tau\sigma z)^2 + 2\tau^2\sigma(1 - \sigma^2)^{1/2}\, rz \cos\phi\right\} \qquad (44)$$

It is straightforward to show that p' is identical with the reduced pressure p_b in the body-fixed system for the same point. The difference p - p' has to be taken into account in calculating forces normal to the cylinder walls and for the moments

perpendicular to the z-axis. No contribution is made to the despin moment about the z-axis, that arises from only tangential shear stresses on the walls.

5. LINEARIZED EQUATIONS

The momentum equation [see equation (39)] is nonlinear due to the convective terms contained in D'. There is little hope of finding solutions of the full system equations [see equations (38) through (41)] except approximations from computational or perturbation methods. Perturbation methods often enhance insight into the structure of the problem and, therefore, we consider in this section the lowest-order approximation for small deviations v_r, v_ϕ, v_z, p' from rigid-body motion, small enough for neglecting the quadratic nonlinear terms.

There are two circumstances that lead to small deviations. The first case of weak forcing through Ω_r was mentioned above. The second case occurs at a small Reynolds number, that is, large viscous damping. The motion is then essentially governed by the terms multiplied by 1/Re in equation (39). We will consider this case in Section 5.3

5.1 The Case of Weak Forcing.

According to equations (39) and (36), weak forcing occurs for

$$\tau\sigma << 1 \qquad (45)$$

This condition can be satisfied by either small τ (nutation rate small in comparison with the spin rate) or small σ (small nutation angles), or a mixture of both. It is not necessary to restrict and σ separately as was done in some previous studies.[21]

With equation (45) satisfied and velocity components of order $O(\tau\phi)$, equations (39) can be reduced to

$$\frac{\partial v_r}{\partial t} + \frac{\partial v_r}{\partial \phi} - 2(1 + \Omega_z)\, v_\phi$$

$$= - \frac{\partial p'}{\partial r} + \frac{1}{Re}\left[D''v_r - \frac{v_r}{r^2} - \frac{2}{r^2}\frac{\partial v_\phi}{\partial \phi}\right] \tag{46a}$$

$$\frac{\partial v_\phi}{\partial t} + \frac{\partial v_\phi}{\partial \phi} - 2(1 + \Omega_z)\, v_r$$

$$= - \frac{1}{r}\frac{\partial p'}{\partial \phi} + \frac{1}{Re}\left[D''v_\phi - \frac{v_\phi}{r^2} + \frac{2}{r^2}\frac{\partial v_r}{\partial \phi}\right] \tag{46b}$$

$$\frac{\partial v_z}{\partial t} + \frac{\partial v_z}{\partial \phi} = - \frac{\partial p'}{\partial z} - 2r\Omega_r + \frac{1}{Re} D''v_z \tag{46c}$$

Continuity equation (38) and boundary conditions equation (41) remain unchanged. This system of equations is linear, but of high order due to the presence of viscous terms. It is the key to understanding the moments exerted at the cylinder for arbitrary Reynolds number and weak forcing. The steady solutions at small values of Re are of special interest. A first attempt to find these solutions in closed form led to yet unresolved problems with the boundary conditions for a finite-length cylinder. We return to this point in Section 5.3. Only for small viscosity, that is, for the limit $Re \to \infty$, the system equations (38), (46), and (41) allow for relatively simple solutions.

5.2 The Inviscid Limit.

For $Re \to \infty$ and equation (45), continuity equation and momentum equations take the following form:

$$\frac{1}{r}\frac{\partial}{\partial r}(rv_r) + \frac{1}{r}\frac{\partial v_\phi}{\partial \phi} + \frac{\partial v_z}{\partial z} = 0 \qquad (47a)$$

$$\frac{\partial v_r}{\partial t} + \frac{\partial v_r}{\partial \phi} - 2(1 + \Omega_z)\, v_\phi = -\frac{\partial p'}{\partial r} \qquad (47b)$$

$$\frac{\partial v_\phi}{\partial t} + \frac{\partial v_\phi}{\partial \phi} + 2(1 + \Omega_z)\, v_r = -\frac{1}{r}\frac{\partial p'}{\partial \phi} \qquad (47c)$$

$$\frac{\partial v_z}{\partial t} + \frac{\partial v_z}{\partial \phi} = -\frac{\partial p'}{\partial z} - 2r\Omega_r \qquad (47d)$$

This system is similar to that considered by Stewartson and Roberts, who neglected Ω_z.[21] Using an ansatz of the form

$$v_r = f_r(r,z)\sin(\phi + kt),\ v_\phi = f_\phi(r,z)\cos(\phi + kt)$$

$$v_z = f_z(r,z)\sin(\phi + kt),\ p' = g(r,z)\cos(\phi + kt) \qquad (48)$$

one obtains

$$(1 + k)\, f_r - 2(1 + \Omega_z)\, f_\phi = -\frac{\partial g}{\partial r} \qquad (49a)$$

$$-(1 + k)\, f_\phi + 2(1 + \Omega_z)\, f_r = \frac{1}{r}\, g \qquad (49b)$$

$$(1 + k)\, f_z = -\frac{\partial g}{\partial z} + 2r\,\frac{\tau\alpha\cos\phi}{\cos(\phi + kt)}\,.^{21} \qquad (49c)$$

The first two equations provide

$$f_r = \frac{\left[-(1 + k)\frac{\partial g}{\partial r} - 2(1 + \Omega_z)\frac{g}{r}\right]}{(1 + k)^2 - 4(1 + \Omega_z)^2} \qquad (50a)$$

$$f\phi = \frac{\left[-2(1 + \Omega_z)\frac{\partial g}{\partial r} - (1 + k)\frac{g}{r}\right]}{(1 + k)^2 - 4(1 + \Omega_z)^2} \tag{50b}$$

Continuity equation (47a) requires

$$\frac{\partial^2 g}{\partial r^2} + \frac{1}{r}\frac{\partial g}{\partial r} - \frac{g}{r^2} + \frac{(1 + k)^2 - 4(1 + \Omega_z)^2}{(1 + k)^2}\frac{\partial^2 g}{\partial z^2} = 0 \tag{51}$$

which can be written as a Laplace equation for g, by suitably transforming z. A particular steady solution of equation (51) for $k = 0$ can be found in the form

$$g_0 = Arz + Br,\ p_0' = g_0 \cos\phi \tag{52}$$

Consequently

$$v_{r_0} = \frac{(Az + B)\sin\phi}{1 + 2\Omega_z},\quad v_{\phi_0} = \frac{(Az + B)\cos\phi}{1 + 2\Omega_z}$$

$$v_{z_0} = (2\tau\sigma - A)\, r \sin\phi \tag{53}$$

This solution accounts for the steady forcing term in equation (49c). Additional unsteady solutions with $k \neq 0$ can be found from equations (49), (50), and (51) with the forcing term in equation (49c) dropped. These unsteady solutions represent the modes of inertial oscillations. Under more restrictive conditions, these modes were studied by Stewartson for a cylindrical container, and by Stewartson and Roberts for a spheroidal container.[11,21] The spheroidal container is an interesting special case where only one mode of oscillation of the liquid is induced by nutation.

For the spheroidal container with aspect ratio λ

$$r^2 + \frac{z^2}{\lambda^2} = 1 \tag{54}$$

considered by Stewartson and Roberts, the boundary conditions can be written in the form

$$rv_r + \frac{zv_z}{\lambda^2} = 0 \tag{55}$$

It follows that B = 0 in equation (53), but

$$A = 2\tau\sigma(1 + 2\Omega_z)/(1 + 2\Omega_z - \lambda^2) \tag{56}$$

The unsteady solutions are free oscillations of arbitrary amplitude C, which is fixed by initial conditions and frequency:

$$k = \frac{1 + 2\Omega_z - \lambda^2}{1 + \lambda^2} \cdot \tag{57}$$

If container shape λ and nutation rate and angle are such that $k \neq 0$, the solution is

$$v_r = \frac{2\Omega_\phi z}{1 + 2\Omega_z - \lambda^2} + Cz \sin(\phi + kt)$$

$$v_\phi = \frac{-2\Omega_r z}{1 + 2\Omega_z - \lambda^2} + Cz \cos(\phi + kt)$$

$$v_z = \frac{-2\lambda^2\Omega_\phi r}{1 + 2\Omega_z - \lambda^2} - C\lambda^2 r \sin(\phi + kt)$$

$$p' = \frac{-2(1 + 2\Omega_z)\,\Omega_r rz}{1 + 2\Omega_z - \lambda^2}$$

$$+ 2C\,\frac{\lambda^2(1 + \Omega_z)}{1 + \lambda^2}\,rz\cos(\phi + kt) \qquad (58)$$

For a sphere, $\lambda = 1$, the frequency from equation (57) is $k = \Omega_z$. This result is different from Stewartson and Roberts, who found resonance, $k = 0$ for $\lambda = 1$. This result is reproduced by letting $\Omega_z \to 0$ in equations (57) and (58).

Here, resonance occurs in a slightly nonspherical container with $\lambda^2 = 1 + \Omega_z$. For $k = 0$, we obtain a solution in the form

$$v_r = \frac{Az}{1 + 2\Omega_z}\sin\phi - \frac{\Omega_r}{1 + \Omega_z}\,zt$$

$$v_\phi = \frac{Az}{1 + 2\Omega_z}\cos\phi = \frac{\Omega_\phi}{1 + \Omega_z}\,zt$$

$$v_z = -Ar\sin\phi + \frac{(1 + 2\Omega_z)\,\Omega_r}{1 + \Omega_z}\,rt$$

$$p' = Azr\cos\phi + \frac{zr}{1 + \Omega_z}\left[\Omega_r - (1 + 2\Omega_z)\,\Omega_\phi t\right] \qquad (59)$$

where A is an arbitrary constant governed by the initial conditions. The physical interpretation of the solutions [see equations (58) and (59)] is very similar to that given by Stewartson and Roberts.

Disregarding the constants in these solutions, which are as yet undetermined, we find that velocity components and the

pressure p' are proportional to $\tau\sigma$, or of order $0(\tau\sigma)$. We also note the Simple periodicity of the solution in the azimuthal coordinate ϕ.

5.3 Effect of Viscosity.

We have not yet found analytical solutions of the viscous equations (46) subject to equations (38) and (41). With the solutions of the previous section and those of Stewartson for the inviscid case, however, we can obtain some qualitative information on viscous solutions.[11] The inertial oscillations will suffer increased damping as the Reynolds number decreases. The resonant peaks in the side moments versus τ will broaden and finally perish. At a sufficiently low Reynolds number, the equations support a steady solution. The dependence of this solution on ϕ will still be simple. However, the simultaneous appearance of velocity components and their derivatives with respect to ϕ in equation (46), for example, $\partial v_r/\partial\phi$ and $-v_r/(Re \cdot r^2)$ in equation (46a) indicates a phase shift of the velocity field with respect to the forcing. This shift increases as Re decreases.

Exploiting the simple periodicity in ϕ, the linearized equations can be reduced to partial differential equations for functions of r and z. A separable solution can be found only for an infinite cylinder, $\lambda \to \infty$. We have not pursued this solution for two reasons. First, it is questionable whether this solution is relevant to the problem with $\lambda = 0(1)$. Second, the solution of the resulting ordinary differential equation plus boundary conditions requires a major computational effort. For finite aspect ratios, the main difficulty for the analytical work is to satisfy the boundary conditions at side walls and end walls simultaneously. Similar problems were found by Gerber, Sedney, and Bartos.[14] They employed the boundary-layer approximation in order to satisfy the no-slip condition at the end walls. Therefore, the range of applicability of their method is comparable to Murphy's method, which uses the boundary-layer approximation at end walls and side

walls.[13] These methods are not applicable at low Reynolds numbers where viscous boundary-layers thicken and finally merge, overwhelming the inviscid core. For this viscous range, further analytical work needs to be carried out. Alternatively, the partial differential equations for the functions of r and z can be solved by computational methods. The problem of solving the linearized equations appears as a basically two-dimensional special case of the full problem based on the nonlinear equations in Section 4.2

5.4 Scaling Aspects.

From equations (38), (41), and (46), we have made various attempts to obtain modified systems of equations that reveal the functional dependence on combinations of the dimensionless parameters. We have not yet been successful in identifying single (or paired) parameter combinations that govern the solution. The dependence on λ concealed in the boundary conditions can be introduced into the differential equations by stretching the z-axis, $z = \lambda\tilde{z}$. In order to keep the continuity equation free from parameters, the axial velocity can be replaced by $v_z = \lambda\tilde{v}_z$. The parameters τ and σ introduced by the forcing term in equation (46c) can be incorporated in the velocity scale. The form of λ_ϕ in equations (53) or (58) suggests rescaling the velocity components and pressure p' by a factor $\lambda\tau\sigma$, which would replace the reference velocity ωa by $\Omega c \sin\Theta$. We note, however, that no change of the Reynolds number would occur in the linear equations for the deviation from rigid-body rotation. Additional information on proper scaling is expected from pursuing analytical solutions of these equations.

5.5 Estimates on the Velocity.

In order to obtain some guidance on the validity of the linearized equations, we consider Miller's experimental data, in particular his figure 13.[6] With $\Theta = 20°$ we obtain $\sigma = 0.342$, while

τ varies between 0.125 and 0.25. Therefore, $0.043 \leq \tau\sigma \leq 0.086$, which can be considered small. It is questionable, however, whether the resulting deviations from rigid-body motion are small enough for linearization. With $\lambda = 4.29$, the inviscid forced solution scales with $\lambda\tau\sigma \leq 0.367$, which may be too large to permit use of equation (46). On the other hand, viscous damping will reduce the deviation.

The measured despin moments allow a rough estimate of the velocity gradients at the cylinder walls. These moments originate from the shear stresses $\tau_{r\phi}$, at the side wall, and $\tau_{z\phi}$, at the end walls. We assume that $\tau_{z\phi}$ and $\tau_{r\phi}$ are of the same order and can be replaced by an average value $\bar{\tau}$. The despin moment can then be written as

$$M = \bar{\tau} \cdot 4\pi a^3 \left(\lambda + \frac{1}{3}\right) \tag{60}$$

The term 1/3 represents the contribution from the end walls and can be dropped in comparison with $\lambda = 4.29$, so that equation (60) contains only the average of $\tau_{r\phi}$ for $r = a$. This stress is defined as

$$\tau_{r\phi}\Big|_{r=a} = \nu\rho\left[\frac{1}{r}\frac{\partial v_r}{\partial \phi} + \frac{\partial v_\phi}{\partial r} - \frac{v_\phi}{r}\right]_{r=a} \tag{61}$$

With $v_r = v_\phi = 0$ at the side wall, we obtain

$$\bar{\tau} = \left|\overline{\tau_{r\phi}}\right|_{r=a} = \nu\rho\left|\overline{\frac{\partial v_\phi}{\partial r}}\right|_{r=a} \tag{62}$$

Exploiting equation (60), the average gradient of v_ϕ at the side wall can be expressed as

$$\bar{v}/a = \left| \overline{\frac{\partial v_\phi}{\partial r}} \right|_{r=a} = \frac{M}{4\pi a^3 \lambda \rho \nu} \tag{63}$$

With $M \simeq 0.7$ N · m for $\nu = 1$ m^2/sec, and $\rho = 1400$ kg/m^3, the average velocity gradient is $\bar{v}/a = 0.04$/sec, providing an average velocity of the order $\bar{v} = 0.002$ m/sec. The dimensionless value with respect to the angular velocity of the rigid-body rotation ($\omega = 3000$ rpm) is $\bar{v}/(\omega a) = 0.00013$, very small indeed. For $\nu = 0.01$ m^2/sec, the values are $\bar{v}/a = 8.5$/sec, $\bar{v} = 0.5$ m/sec, $\bar{v}/(\omega a) = 0.027$, still sufficiently small to allow using the linear equations. Therefore, the linear equations seem to cover the full range where large despin moments were observed. For the smaller viscosity $\nu = 10^{-4}$ m^2/sec, the velocity gradient assumes a large value, $\bar{v}/a = 254$/sec. Formally, we obtain $\bar{v} = 15.3$ m/sec. This number may be misleading, however, since the growth of the velocity occurs only across the thickness $\sigma < a$ of the viscous boundary layer. The estimates from equation (63) provide some guidance on the magnitude of the velocity only in the fully viscous regime, say for Reynolds numbers Re < 1000.

6. REMARKS ON MORE GENERAL CASES

From the foregoing discussion, it appears that the viscous fluid motion in the spinning and nutating cylinder can be studied on the basis of the linearized equations of Section 5. However, there are a number of disconnected topics that require using other sets of equations. Concerning the gyroscope experiments and the still unexplained changes in the yaw angle growth rates, the solutions of the inviscid equations should be reconsidered without resorting to weak forcing [equation (45)]. Beyond the inertial modes studied by Stewartson, which have period 2π in ϕ, other classes of modes exist with period $2\pi/n$, $n > 1$, which may be excited through the generation of harmonics at larger yaw angles.[11]

Other cases of interest are the viscous fluid motions at smaller spin rates, where equation (45) may not be satisfied. Whenever equation (45) is invalid, the products of Ω_r and Ω_ϕ with velocity components in equation (39) must be retained. Even at a small Reynolds number, these products generate harmonics in ϕ, and the flow field assumes the form of a Fourier series in ϕ.

Only the linearized equations of Section 5 bear the promise of analytical or, at least, semianalytical solutions. Strong forcing or large deviations from rigid-body motion can only be treated by numerical methods. There is as yet, little experience in computing internal flows in simply connected rotating containers. The three problem areas that need to be overcome are

- No-slip condition at the end walls
- Three-dimensionality of the flow field
- Failure of most methods at the axis r=0.

As mentioned above, use of the linearized equations reduces the problem to two dimensions, r and z. We have studied the applicability of three classes of methods--finite difference, polynomials, and finite element.

Finite-difference methods seem to be least promising due to the difficulty of achieving sufficient accuracy in presence of the axis at r = 0. The simple geometry of the cylinder favors using spectral methods, with a Fourier expansion in ϕ and a Chebyshev expansion in z. Use of Chebyshev polynomials in r was considered, but abandoned for slow convergence of the series. Legendre polynomials or Jacobi polynomials in r appear as the better choice, but additional numerical studies are necessary for evaluating the convergence properties. Whereas polynomials are usually chosen for computational ease, expansions in Bessel functions may work best for the present problem. It requires, however, major efforts to

develop this yet-unexplored branch of spectral expansions. The third method that seems most straightforward to apply to the present problem is a finite-element method. No difficulties are encountered on the axis. Even for the three-dimensional problem, a relatively small number of elements may provide sufficient accuracy of the moments. The accurate calculation of the flow field with a large number of elements is a straightforward extension at increased computational expense.

Blank

LITERATURE CITED

1. D'Amico, W.P. Ballistic Research Laboratory Memorandum Report 2791. Early Flight Experiments with the XM761. September 1977.

2. D'Amico, W.P. Ballistic Research Laboratory Memorandum Report 2792. Field Tests of the XM761: First Diagnostic Test. AD B0249760. September 1977.

3. D'Amico, W.P. Ballistic Research Laboratory Memorandum Report ARBRL-MR-02806. Field Tests of the XM761: Second Diagnostic Test. AD B025305L. January 1978

4. Miller, M.C. ARCSL-SP-79005. Flight Instability Test Fixture for Nonrigid Payloads. January 1979.

5. Miller, M.C. Flight Instabilities of Spinning Projectiles Having Nonrigid Payloads. American Institute of Aeronautics and Astronautics Paper 810223. January 1981.

6. Miller, M.C. Flight Instabilities of Spinning Projectiles Having Nonrigid Payloads. J. Guidance, Control, and Dynamics 5, 151-157 March - April (1982).

7. Vaughn, H.R. Flight Dynamic Instabilities of Fluid Filled Projectiles. Sandia National Laboratories, SAND 78-0999. January 1978.

8. Miller, M.C. Void Characteristics of a Liquid-Filled Cylinder Undergoing Spinning and Coning Motion. J. Spacecraft and Rockets 18 (No. 3), 287-288 May - June (1981).

9. Miller, M.C. Experimental Measurement of the Flow Field in a Liquid-Filled Cylinder Undergoing Simultaneous Spinning and Coning Motion. ARRADCOM Aeroballistics and Fluid Dynamics 1982 Research and Technology Conference, Downingtown, PA. September 1982.

10. D'Amico, W.P., and Rogers, T.H. Yaw Instabilities Produced by Rapidly Rotating, Highly Viscous Liquids. American Institute of Aeronautics and Astronautics Paper 81-0224. January 1981.

11. Stewartson, K. On the Stabilities of a Spinning Top Containing Liquid. J. Fluid Mechanics 5 (Part 4), 577-592 June (1959).

12. Wedemeyer, E.H. Ballistic Research Laboratory Report 1325. Viscous Corrections to Stewartson's Stability Criterion. AD 4896587. June 1966.

13. Murphy, C.H. Ballistic Research Laboratory Memorandum Report ARBRL-MR-03194. Angular Motion of a Spinning Projectile with a Viscous Liquid Payload. August 1982.

14. Gerber, N., Sedney, R., and Bartos, F.M. Ballistic Research Laboratory Technical Report ARBRL-TR-0242. Pressure Moment on a Liquid-Filled Projectile: Solid Body Rotation. 1982.

15. Karpov, B.G. Ballistic Research Laboratory Report 1279. Dynamics of Liquid-Filled Shell: Resonance and Effect of Viscosity. AD468054 1965.

16. Scott, W.E , and D'Amico, W.P. Amplitude-Dependent Behavior of a Liquid-Filled Gyroscope. J. Fluid Mechanics 60 (Part 4), 751-758 (1973).

17. Scott, W.E. The Large Amplitude Motion of a Liquid-Filled Gyroscope and the Non-Interaction of Inertial and Rossby Waves. J. Fluid Mechanics 72 (Part 4), 649-660 (1975).

18. Gortler, H. Dimensionsanalyse. Springer-Verlag, Berlin. 1975.

19. Vaugl , H.R. Sandia National Laboratories, SC-M-67-2933. A Detailed Development of the Tricylic Theory. February 1968.

20. Pedloski, F. Geophysical Fluid Dynamics. Springer-Verlag, Berlin. 1979.

21. Stewartson, K. and Roberts. On the Motion of a Liquid in a Spheroidal Cavity of a Precessing Rigid-body. J. Fluid Mechanics 17, 1-20 (1963).